Quantifying the influences of atmospheric stability on air pollution in Lanzhou, China, using a radon-based stability monitor

Scott D. Chambers [a], Fenjuan Wang [b, c, *], Alastair G. Williams [a], Deng Xiaodong [d], Hua Zhang [b], Giovanni Lonati [c], Jagoda Crawford [a], Alan D. Griffiths [a], Antonietta Ianniello [e], Ivo Allegrini [f]

[a] *Institute for Environmental Research, ANSTO, Locked Bag 2001, Kirrawee DC, NSW 2232, Australia*
[b] *Laboratory for Climate Studies, National Climate Center, China Meteorological Administration, Beijing 100081, China*
[c] *Department of Civil and Environmental Engineering, Politecnico di Milano, Milan 20133, Italy*
[d] *Lanzhou Environmental Monitoring Center, Lanzhou 730000, Gansu, China*
[e] *Institute of Atmospheric Pollution Research, National Research Council, 00016 Monterotondo Stazione, Rome, Italy*
[f] *Research Consortium CORAM, Pastorano, CE, Italy*

Received 28 November 2014
Received in revised form
3 February 2015
Accepted 5 February 2015
Available online 7 February 2015

* Corresponding author. Laboratory for Climate Studies, National Climate Center, China Meteorological Administration, Beijing 100081, China.
E-mail address: wangfj@cma.gov.cn (F. Wang).

1. Introduction

The dramatic economic expansion in China in recent decades has relied heavily upon the use of fossil fuels, primarily coal combustion (about 70%), which has led to huge increases in pollutant emissions. China is now facing the worst air pollution problem in its recorded history (Chan et al., 2008; Kan et al., 2012; Zhang et al., 2012a). According to 2013 Chinese Environmental Reports, ambient air quality levels meet the country's new standards in only 3 of the 74 major Chinese cities (Ministry of Environmental Protection of People's Republic of China (2014)). Pollutant concentrations for 2013, averaged across all major cities, included: 72 $\mu g/m^3$ for $PM_{2.5}$, 118 $\mu g/m^3$ for PM_{10} and 44 $\mu g/m^3$ for NO_2 (Chinese Ministry of Environmental Protection (2014)). Severe pollution events such as haze are common (He et al., 2011; Ji et al., 2014), and particulate matter from these episodes can be transported long distances within China (e.g. Nie et al., 2013; Zhang et al., 2014) and beyond (e.g. Jo and Kim, 2013; Begum et al., 2011; Ohara et al., 2007; Park et al., 2004; Huebert et al., 2003; Guttikunda et al., 2001). A clearer understanding of the variability in near-surface concentrations of primary and secondary pollutants throughout the major Chinese cities is essential for estimating public health impacts, identifying the need for (and assessing the efficacy of) emission mitigation strategies, as well as improving the predictive abilities of chemical transport models. In few regions is this task more challenging than Lanzhou, where mean nocturnal wind speeds representative of well-mixed and poorly-mixed conditions differ by only 0.4 m s^{-1}.

Pollutant concentrations in the atmospheric boundary layer (ABL) are a complex function of many factors, including: source strengths and distribution, local meteorology and chemistry (e.g. Chambers et al., 2014b; Perrino et al., 2001; Duenas et al., 1996). On short (sub-diurnal) timescales the extent of the vertical column within which emissions mix often has the largest influence on measured concentrations, and the depth of this mixing volume is in turn closely related to the thermal stability of the ABL. The fundamental connection between atmospheric stability and pollution exceedance events has long been established (e.g. Wang et al., 2013a; Ji et al., 2012; Zhang et al., 2012b; Di Carlo et al., 2007; Desideri et al., 2006; Galmarini, 2006; Avino et al., 2003; Sesana et al., 2003; Perrino et al., 2001) and a number of meteorology-based techniques are in common use to quantify the "stability" of (or degree of mixing within) the lower atmosphere. These range from simple categorical schemes based on routinely available sur-face meteorological measurements (e.g. Pasquil-Gifford turbulence and radiation schemes: Pasquil, 1961; Turner, 1964; Pasquill and Smith, 1983), to more accurate techniques based on surface and boundary layer similarity theory (e.g. Foken, 2008) which require sophisticated (research quality) instrumentation that is typically expensive and labour intensive. Even the most specialised meteorological stability measures can become problematic when predicting pollution levels accurately in very stable conditions, however, and this is particularly true in challenging geographical and topographical terrain (Acevedo and Fitzjarrald, 2003; Mahrt et al., 2001). Alternative tools for quantification of near-surface atmospheric mixing that are closely matched with pollution transport processes at the surface are needed. Ubiquitous surface-emitted passive natural tracers with simple distributed source and sink functions are candidates, of which atmospheric Radon-222 is rapidly gaining acceptance (e.g. Chambers et al., 2014b; Kondo et al., 2014; Pitari et al., 2014; Williams et al., 2013; Wang et al., 2013b; Perrino et al., 2001; Di Carlo et al., 2007; Sesana et al., 2006; Galmarini, 2006; Desideri et al., 2006; Avino et al., 2003; Duenas et al., 1996; Allegrini et al., 1994; Guedalia et al., 1980).

Radon-222 (radon) is a naturally occurring, unreactive, radioactive gas that is poorly soluble in water. To a good approximation it is derived solely from ice-free, unsaturated land surfaces (soil and rocks), and its only atmospheric sink is radioactive decay (Zahorowski et al., 2004 and references therein). Radon's half-life (3.82 d) is long enough for it to be considered a conservative tracer over the course of a single night, yet short enough that it does not accumulate in the atmosphere on timescales of more than two weeks. These characteristics make radon an ideal tracer of near-surface atmospheric transport and mixing processes (e.g. Williams et al., 2013; Chambers et al., 2009, 2014b). A number of direct and indirect detectors for atmospheric radon are presently available, with a range of measurement frequencies, precision and lower limits of detection to suit a broad range of applications (e.g. Chambers et al., 2014a; Wada et al., 2010; Weller et al., 2013; Perrino et al., 2001; Allegrini et al., 1994).

As diurnal variations in radon concentrations in the lower atmosphere over land represent a direct measure of the effects of vertical mixing on a ubiquitous passive tracer (Williams et al., 2013), they have the potential to generate better predictors for the likelihood of high pollution levels near the surface than the more commonly used (meteorology-based) stability schemes. However, with only a few exceptions (notably Perrino et al., 2001, Perrino, 2012; Chambers et al., 2014b), most studies that have employed radon as a stability indicator have assumed a direct correspondence between observed absolute concentrations and atmospheric mixing (e.g. Allegrini et al., 1994; Avino et al., 2003; Sesana et al., 2003; Galmarini, 2006; Zhang et al., 2012b; Pitari et al., 2014; Wang et al., 2013b). This practice requires the as-sumptions that the local terrestrial radon flux (pertinent to diurnal forcing) is approximately constant, and that fetch effects (advec-tion) can be neglected. Whilst the first of these assumptions is often reasonable for inland locations, the second is certainly not. Due to its 3.82 day half-life, radon concentration time series have a "memory" of fetch influences for up to two weeks, during which time air masses can travel as far as 10,000 km. In addition, varia-tions in the depth of the capping (subsidence) inversion lead to large changes in scalar dilution in the daytime boundary layer on synoptic to seasonal time scales. For these reasons, and depending on the measurement location, local sources are often not the dominant influence on afternoon radon concentrations near the surface. The characteristic diurnal radon signal, which mainly re-flects the influence of the day−night cycle of vertical mixing in the boundary layer, is superimposed upon these long time-scale vari-ations and must be separated from them before it can be used as an accurate indicator of local stability conditions (Chambers et al., 2014b). Failure to condition the radon time series in this way can lead to difficulties when interpreting results from radon stability studies. For example, correlations between radon and wind speed, NO_x or PM_{10} may be lower than expected when using uncondi-tioned radon observations (e.g. Pitari et al., 2014; Zhang et al., 2012b; Vecchi et al., 2007; Galmarini, 2006), particularly for sites near the coast. Also, long time-scale meandering of the "back-ground" radon concentration may erroneously be attributed to changes in atmospheric mixing state (e.g. Sesana et al., 2003; Vecchi et al., 2007; Wang et al., 2013b). Furthermore, while the accumulation of radon overnight is a good indicator of the depth of the nocturnal inversion layer (e.g. Chambers et al., 2014b; Griffiths et al., 2013; Galmarini, 2006; Sesana et al., 2006; Allegrini et al., 1994), afternoon minimum radon concentrations should not be used as an indicator of the depth of the atmospheric boundary layer without careful consideration of the effects of changes in the radon source function associated with fetch variations over the last two weeks, particularly when trajectories include an oceanic component.

The aim of this study is to demonstrate that a radon-based stability index, derived from *carefully conditioned* measurements using a commercially-available "stability analyser", represents a superior tool to the commonly used Pasquil-Gifford "radiation" scheme for quantitative assessment of the impact of changing atmospheric mixing conditions on near-surface concentrations of a range of anthropogenic pollutants in the complex topographical setting of Lanzhou, China.

2. Sites and methods

2.1. Measurement sites and surrounds

Lanzhou, the capital of Gansu Province (population ~2 million), is located in Northwest China on the narrow floodplain of the Yellow River (Fig. 1). The valley within which the city is located is 1500–1600 m above sea level (a.s.l.), 2–8 km in width, and approximately 35 km long. Regional topographic features include: the Tibetan plateau to the West, Baita mountain to the North (relative elevation of 200–300 m), and Gaolan mountain to the South (relative elevation of 300–500 m). Drag associated with the rugged regional topography retards synoptic-scale winds; combined with the unique basin topography, this results in comparatively calm conditions in the vicinity of Lanzhou for most of the year. Long-term meteorological records indicate a mean annual surface wind speed in Lanzhou of 0.8 m s^{-1}, with calm conditions reported for 62% of the time. In particular, January (mid-winter) has a mean wind velocity of only 0.3 m s^{-1}, with calm conditions 81% of the time (Zhang et al., 2001). Largely as a result of this unusual meteorology, which is not conducive to the dispersion of locally generated emissions, Lanzhou is one of the most polluted cities in China.

Measurements reported in this study were conducted by the Environmental Monitoring Center of Lanzhou from July 2007 to May 2008, at three main sites representative of contrasting emission characteristics: Station B (103°42′21″E, 36°06′59″N; 1526 m a.s.l.), Station C (103°43′32″E, 36°04′30″N; 1512 m a.s.l.) and Station D(1040804800E, 355603400N; 1765 m a.s.l.).

Station B is located to the northeast of the main industrial region of Lanzhou city, in a recreation park of the Anning district (Fig. 1). This station is considered to be representative of pollution exposure in a predominantly residential part of the city. Station C, directly east of the main industrial region, is located in the Qilihe district of mixed commercial and industrial activity as well as residential areas. Since it is adjacent to one of Lanzhou's main arterial roads (Yicheng Road), Station C is also representative of exposure to traffic emissions. Station D is beyond the city limits, 30 km to the southeast of the other two stations, in the countryside of Yuzhoug. It is considered representative of rural areas and the regional "background" pollutant concentrations. Further details of the in-dividual sites and local pollutant sources are given in Wang et al.(2013b). Throughout the measurement period routine climatolog-ical observations were made by the China Meteorological Admin-istration (CMA) at a site closest to Station C (103°52′48″E, 36°03′N).

2.2. Radon measurements

Atmospheric radon progeny measurements were made at Station C using an SM200 "stability monitor" (OPSIS AB, Furulund, Sweden; see also Wang et al., 2013b). Sampling was conducted at a flow rate of 16.7 L min^{-1}, through an inlet 3 m above ground level (a.g.l.), and secular equilibrium was assumed between ambient radon and its progeny. Although the SM200 delivers the short-lived beta activity of radon-daughter aerosols every 2 h, the output was converted to hourly resolution (via linear interpolation) in post-processing to better integrate with the meteorology and pollution observations. Details about the background removal and

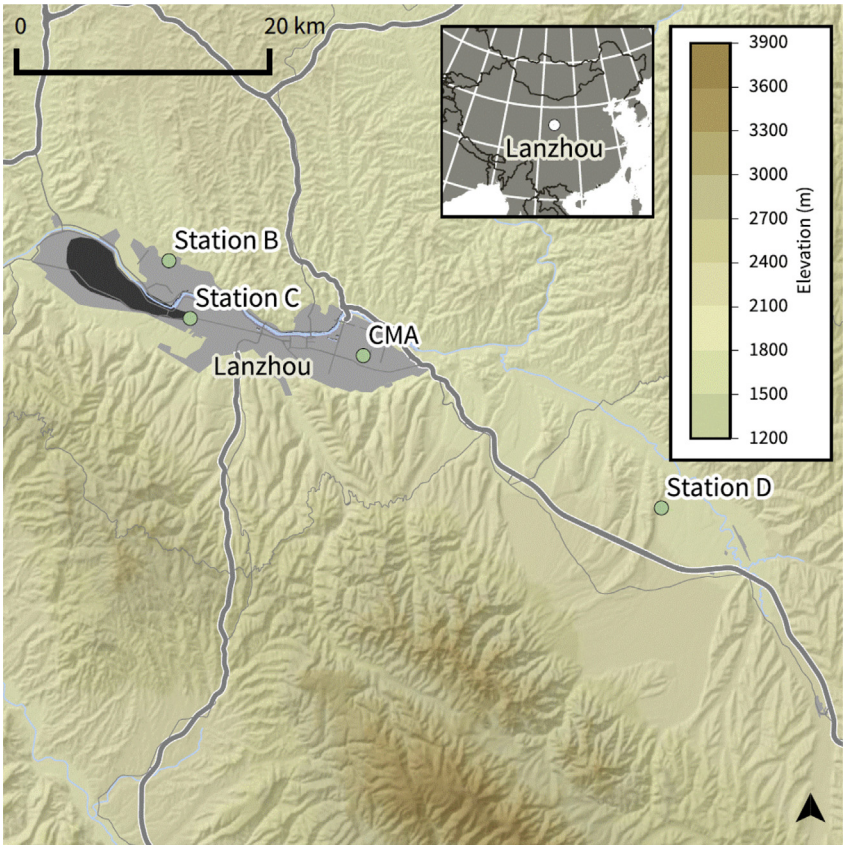

Fig. 1. Location of measurement sites and arterial road network within the Yellow River valley, with inset showing the location of Lanzhou in central China. The main industrial region west of Station C is shaded black, and remaining commercial/residential areas shaded grey.

measurement accuracy of the SM200 are given in Perrino et al. (2001), with further details in Zhang et al. (2012b).

Following exposure of each 2-hr sample filter, the SM200 records beta counts for five 5-min intervals. A curve can then be fitted to these five counts, from which it is possible to determine the mean decay constant and initial activity required to derive a radon progeny concentration. However, for the 2007–2008 Lanzhou ob-servations reported here, only the first of the five 5-min counts (called "Natural[0]") was recorded, so it was not possible to calcu-late absolute radon progeny concentrations. However, subsequent tests have indicated that there is a strong correlation (0.991) be-tween "Natural[0]" and fully calibrated radon progeny concentra-tions. Consequently, throughout the following text, the "Natural[0]" output of the SM200 will be referred to as "Rn*", to denote that it is only a proxy for radon progeny concentrations.

2.3. Pollution and meteorological observations

The gas phase measurement instruments employed include: SO_2 analyser (API 100A) at Stations B and D, a Chemiluminescence NO_x analyser (API 200 A) and a UV absorption ozone analyzer (API 400A) at each station (each of which have a 5 min sampling frequency), CO analyser (API 300E) at stations B and C. Meteorological parameters, including wind speed (m s^{-1}), wind direction (°), relative humidity (%), temperature (°C), solar radiation (W m^{-2}), and atmospheric pressure (hPa), were also measured at Station C.

3. Development of a "stability index" for the SM200

3.1. Refining the Rn* stability signal

Although marketed as a "stability monitor", it is challenging to directly relate the standard output of the SM200 to atmospheric stability in a consistent and quantitative way. Since Rn* is closely related to radon, which has a purely surface terrestrial source, the effect of increasing atmospheric stability (equivalent to reducing the atmospheric mixing volume) within the shallow stable nocturnal boundary layer (SNBL) should be to produce elevated Rn* values. Together with minimum afternoon Rn* values produced by dilution in the much deeper daytime convective atmospheric boundary layer (ABL), these high nocturnal values result in a strong diurnal cycle that is a commonly observed feature of inland radon time series and is clearly apparent in the SM200 output (Fig. 2 black line). However, superimposed upon this diurnal stability-related signal are additional variations in Rn* that can also be large in amplitude (up to 400 units in Fig. 2) but are generally more slowly changing (days to weeks). This additional signal can be seen most clearly by following the variations in afternoon Rn* values, when the atmosphere is most well mixed and ABL depths are maximised (red line in Fig. 2). These additional variations in Rn* are *not* related to local nocturnal atmospheric stability effects, but are a well-known feature of radon time series (e.g. Wang et al., 2013b; Vecchi et al., 2007; Desideri et al., 2006; Galmarini, 2006; Sesana et al., 2006), caused by synoptic to seasonal variations in the large-scale fetch and daytime capping inversion depth (Chambers et al., 2014b, 2009; Zahorowski et al., 2005). In order for the output of the SM200 stability analyser to be used effectively to quantify *only* local stability conditions, it is therefore first necessary to condition the "raw" output time series by isolating contributions to the observed time series on diurnal timescales from those occurring on longer timescales.

As can be seen in Fig. 3, variability in the Lanzhou Rn* record includes contributions on a range of timescales: seasonal, synoptic, diurnal, and hourly. The seasonal Rn* cycle (e.g. Fig. 4a), characterised by a summer minimum and winter maximum, is a result of interplay between several factors, including: seasonal changes in atmospheric mixing depth (daytime and nocturnal), seasonal changes in long-term air mass fetch brought about by the summer/winter Asian monsoons (e.g. Chambers et al., 2009; Zahorowski et al., 2005), and seasonal changes in the strength of the regional radon source function. Since Lanzhou is 1500 km inland, synoptic-scale variability is primarily contributed to by synoptic changes in mixing depth, as well as spatial and temporal variability in the radon source function across Asia (Zhang et al., 2011; Williams et al., 2009; Conen and Robertson, 2002). It is only the diurnal cycle (e.g. Fig. 4b), with amplitudes typically varying from 80 to 380 units (comparable to the amplitude of the monthly median seasonal cycle), that is intimately linked to diurnal changes in atmospheric stability.

On any given afternoon, when ABL depths are maximised, Rn* concentrations are primarily a function of the long-term (2–3 week) fetch history of the air mass. Each evening however, around sunset, a SNBL begins to form from the ground upwards, and beneath the nocturnal inversion the concentration of species with local surface sources begins to evolve independently of values in the residual layer (RL) above that are still dominated by radon from more distant sources.

An approximation of Rn* values above the nocturnal inversion can be made by linearly interpolating between afternoon minimum radon concentrations, as demonstrated in Fig. 2 (red line) employing a routine detailed in Chambers et al. (2014b). This enables a pseudo-gradient measurement to be formed between the near-surface observations and the interpolated Rn* values that are a proxy for observations well-removed from the surface. As evident in Fig. 5, while retaining the details of diurnal variability in Rn*, the gradient data ($\Delta Rn* = Rn*_{observed} - Rn*_{interpolated}$) is largely free from influences on greater than diurnal timescales.

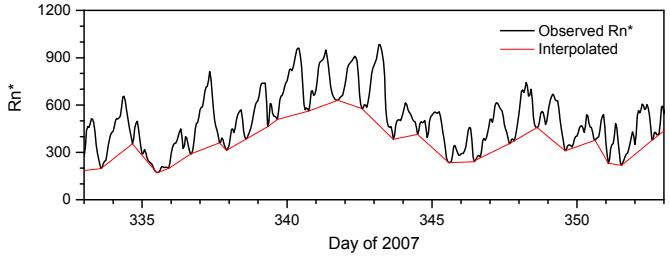

Fig. 2. 20-day subset of SM200 Rn* observations (black line), and an interpolation between afternoon minimum values (red line) adjusted to always be less than, or equal to, the observed Rn*. Units of Rn* are uncalibrated 5-min beta-counts (see Section 2.2 for details). (For interpretation of the references to colour in this figure legend, the reader is referred to the web version of this article.)

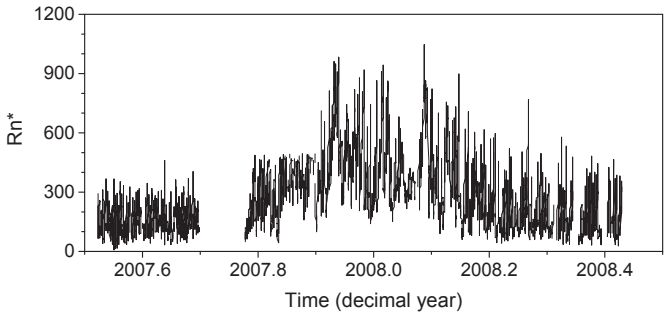

Fig. 3. SM200 Rn* observations at Lanzhou.

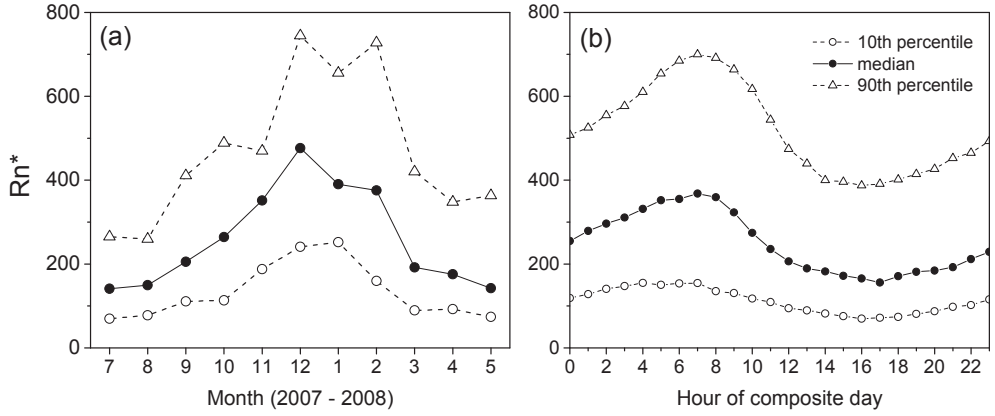

Fig. 4. (a) Monthly distributions of interpolated hourly Rn*, and (b) hourly distributions of Rn* over the diurnal cycle.

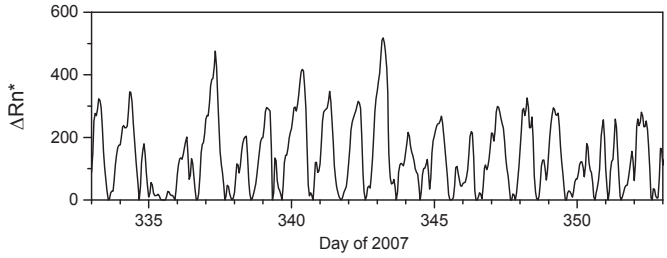

Fig. 5. 20-day subset of the hourly pseudo-gradient, ΔRn*.

3.2. *Defining the stability classification scheme*

Since ΔRn* is primarily a function of diurnal Rn* variability – forced to return each afternoon to the same "reference" (well mixed) value – changes in ΔRn* will be directly relatable to the stability (or mixing state) of the lower atmosphere throughout the night relative to that of the well-mixed daytime atmosphere.

We formed a diurnal composite of ΔRn* (Fig. 6) and defined a 12-h "stability window" that encompassed most of the nocturnal Rn* accumulation period (2 h after average sunset to 2 h after average sunrise). The mean ΔRn* over this window is directly related to the mean atmospheric stability over a whole night relative to the previous daytime conditions.

Next we calculated the mean ΔRn* within the 2000-0800h stability window for every night, and calculated a cumulative frequency histogram of the results (Fig. 7). We then assigned a nocturnal stability category to each of the 4 quartile ranges of the mean windowed ΔRn* values as follows (quartile boundaries indicated in Fig. 7):

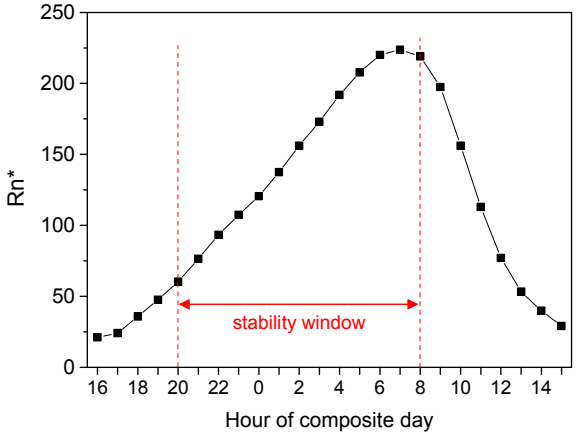

Fig. 6. Diurnal composite ΔRn* showing the 12-h "stability window".

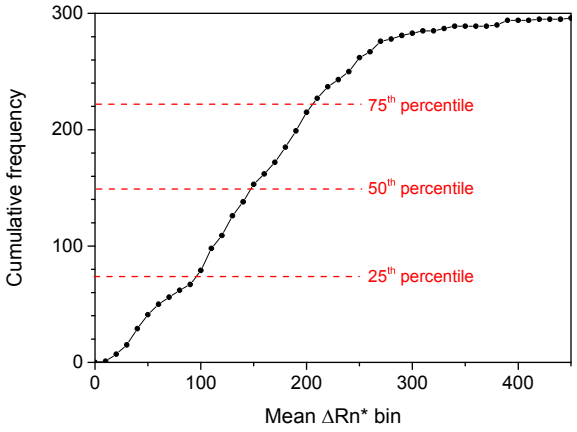

Fig. 7. Cumulative frequency histogram of mean nocturnal ΔRn* in the 2000-0800h stability window.

It is important to note that this kind of classification scheme assigns stability categories relative to conditions typical of the site at which the scheme is defined. That is, since wind speeds at Lanzhou are notoriously low, what constitutes "well mixed" conditions at this site is likely to be quite different from "well mixed" conditions at, for example, a flat exposed site. However, by grouping meteorological quantities by the same classification scheme (see Section 4.3), it is possible to quantify exactly what climatological conditions are typical of each stability class when comparing results between sites.

Furthermore, the choice of four stability categories in Fig. 7 was fairly arbitrary; depending on the length of available observations and requirements of the experiment, a lesser or greater number of

Quartile	Stability category	Vertical mixing
Q1	Near neutral	Well mixed (deep NBL)
Q2	Weakly stable	Moderately mixed
Q3	Moderately stable	Weakly mixed
Q4	Stable Poorly mixed	(shallow NBL)

categories could be chosen, limited primarily by the need to retain enough daily samples within each stability category to obtain statistically sound composite information. Analysis of the 11-month Lanzhou dataset resulted in ~80 samples per category (~20 if considered by season). For this reason, seasonal analyses should ideally be performed on multi-year datasets.

Having assigned one of the four defined stability categories to each night of the Lanzhou Rn* record, we finally formed diurnal composites of Rn* for each of the stability categories (Fig. 8). It is evident that for the 25% (first quartile) of evenings for which the nocturnal atmosphere in the vicinity of Lanzhou was nearly neutral (most well mixed), the diurnal amplitude of ΔRn* was very small (43 units), whilst for the 25% of evenings over which the atmosphere was most stable, the ΔRn* diurnal amplitude was an order of magnitude larger (392 units).

Since the four curves of Fig. 8 are each averages over many (~80) days they represent idealised forms of the respective stability categories. Intermittent mixing events on individual nights will result in deviations from these idealised scenarios but are accounted for by averaging over the nocturnal "stability window" (Fig. 6).

It should be noted that in some exceptional circumstances, such as persistent complete cloud cover over a region covered with snow, that similarly stable atmospheric conditions can persist day and night for prolonged periods and little diurnal cycle in radon concentrations is evident. In such cases the stability classification scheme proposed here would be difficult – if not impossible – to effectively employ. Better results would perhaps be obtained using actual (as opposed to pseudo) gradient measurements, provided the height of the second detector's inlet was well above the height of the stable boundary layer (e.g. 100–200 m).

Under conditions of prolonged atmospheric stagnation, long-lived primary emissions and secondary pollutants (such as some aerosols) can accumulate from day-to-day. Under such circumstances, assuming a diurnal cycle is still discernible, the long timescale ("fetch-related") component of the radon signal should not be discarded after isolation, since it can provide vital information regarding day-to-day accumulation rates (providing appropriate decay corrections are applied).

4. Results and discussion

4.1. Lanzhou climatology

In the Yellow River floodplain, sheltered by substantial topography to the North and South, wind speeds at Lanzhou are low to moderate; mean monthly wind speed over the measurement period ranged from 0.9 to 1.5 m s^{-1} (Fig. 9a), with values of 4–6 m s^{-1} only occasionally recorded. Dominance of the Central Asian anticyclone is evident in the mean monthly pressure record between October and February (Fig. 9d), marking the height of the winter monsoon and long terrestrial air mass fetches across continental Asia, as seen in the Rn* record (Figs. 3 and 4a). Mean temperatures jump from February to March (Fig. 9c), a sign of the transition from winter to summer monsoonal conditions, also indicated by the change in dominant wind direction (Fig. 9b).

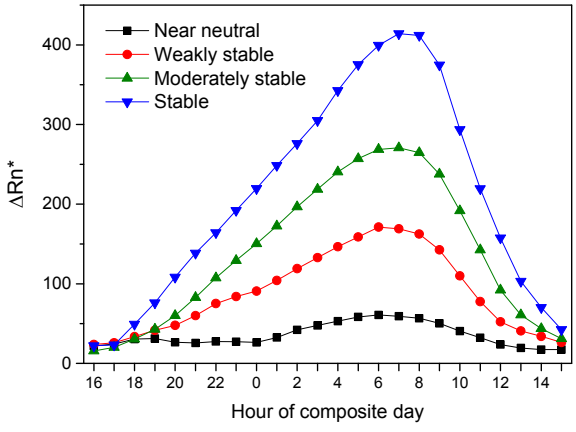

Fig. 8. Mean diurnal cycles of ΔRn* for four arbitrarily defined nocturnal stability categories at Lanzhou.

Monthly-mean (a) diurnal (ΔRn*), and (b) fetch-related (Fig. 2 red line) contributions to the Rn* signal are presented in Fig. 10. ΔRn* values (a proxy for nocturnal stability) show only a minor seasonal variability, being greatest from October through February, when wind speeds are at or below the annual average, temperatures are generally below the annual average, and subsidence within the Asian anticyclone frequently results in clear-sky nights (Fig. 9). The purely fetch-related contribution to the Rn* observations (Fig. 10b) exhibits a much stronger seasonal signal, however, bearing a strong resemblance to the overall seasonal Rn* cycle of Fig. 4a; highlighting the significance of fetch effects in shaping the seasonal Rn* cycle.

4.2. Climatology of defined stability categories

Using the radon-based stability categories defined in Section 3.2 (i.e. completely independently of the climatological observa-tions), we formed diurnal composites of the Lanzhou wind speed and temperature records (Fig. 11). Despite the unusually low range of wind speeds observed at this site, the radon-based classification scheme is able to clearly distinguish small changes in mean wind conditions between the different stability classes. The most well-mixed days (referred to here as "near neutral") exhibited the highest daily mean wind speeds (1.4 m s^{-1}), and lowest diurnal amplitude of temperature (6.2 °C). Stable nights were characterised by the lowest wind speeds for the first half of the night, and steepest temperature gradients shortly after sunset and sunrise.

The increase in wind speed for stable and moderately stable cases noted from 0100h until sunrise is likely attributable to katabatic drainage flows from the surrounding topography. Density currents that enter the valley from the North and South will eventually flow "downstream" (West to East) along the floodplain, taking with them some of the accumulated emissions. Since the measurement sites are located East of the industrial region of the city, most of the emissions should still be observed. However, given the disparity in spatial distribution of sources for radon and anthropogenic emissions, and the meandering nature of drainage flows, correlations between nocturnal accumulation of radon and pollution at this site may be less than optimal under the most stable of conditions.

The most stable nights were usually associated with clear-sky conditions and, in the following mornings, the clear-sky conditions usually resulted in the strongest convective mixing and valley circulation; as evident from the higher wind speeds between 1100 and 1400h on days that have stable nocturnal conditions (blue triangles, Fig. 11a), and most rapid increases in morning temperature.

4.3. Implementing the stability classification scheme for selected pollutants

We formed diurnal composite hourly means of SO_2, CO, NO and NO_2 at each site for the four stability categories using the whole dataset (Fig. 12). Clearly, the radon-based classification

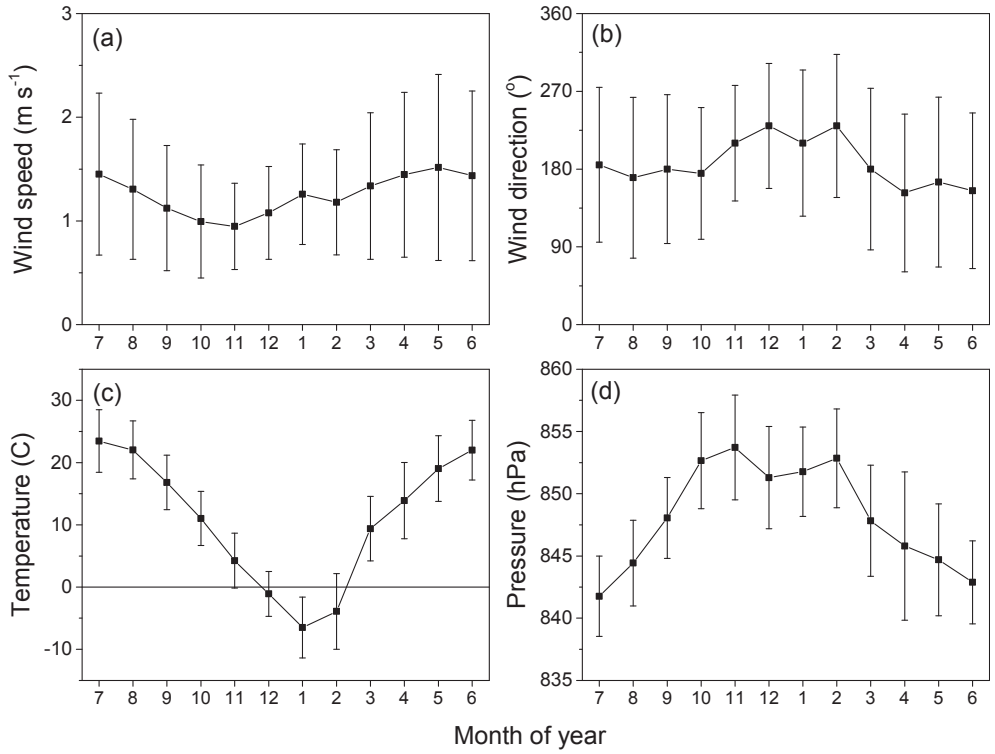

Fig. 9. Summary of Lanzhou climatology between July 2007 and June 2008. Filled circles represent monthly means and whiskers ±1σ.

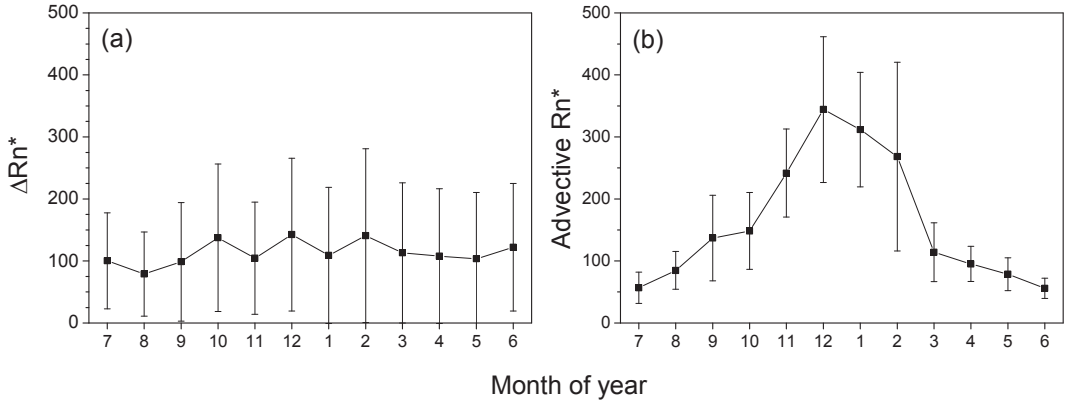

Fig. 10. Mean monthly (a) diurnal, and (b) fetch-related, contributions to annual Rn* observations. Filled squares represent monthly means and whiskers denote ±1σ.

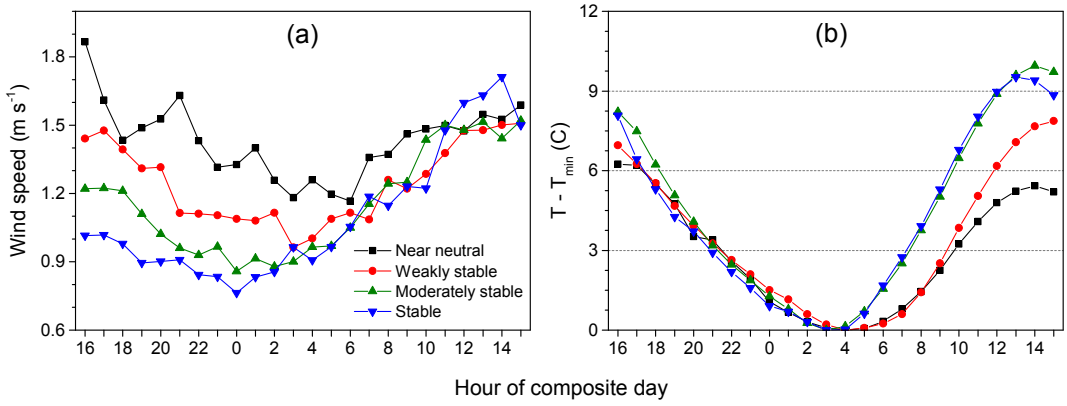

Fig. 11. Hourly-mean diurnal composites of (a) wind speed, and (b) temperature range (daily minimum removed: $T - T_{min}$), as a function of radon-based stability category.

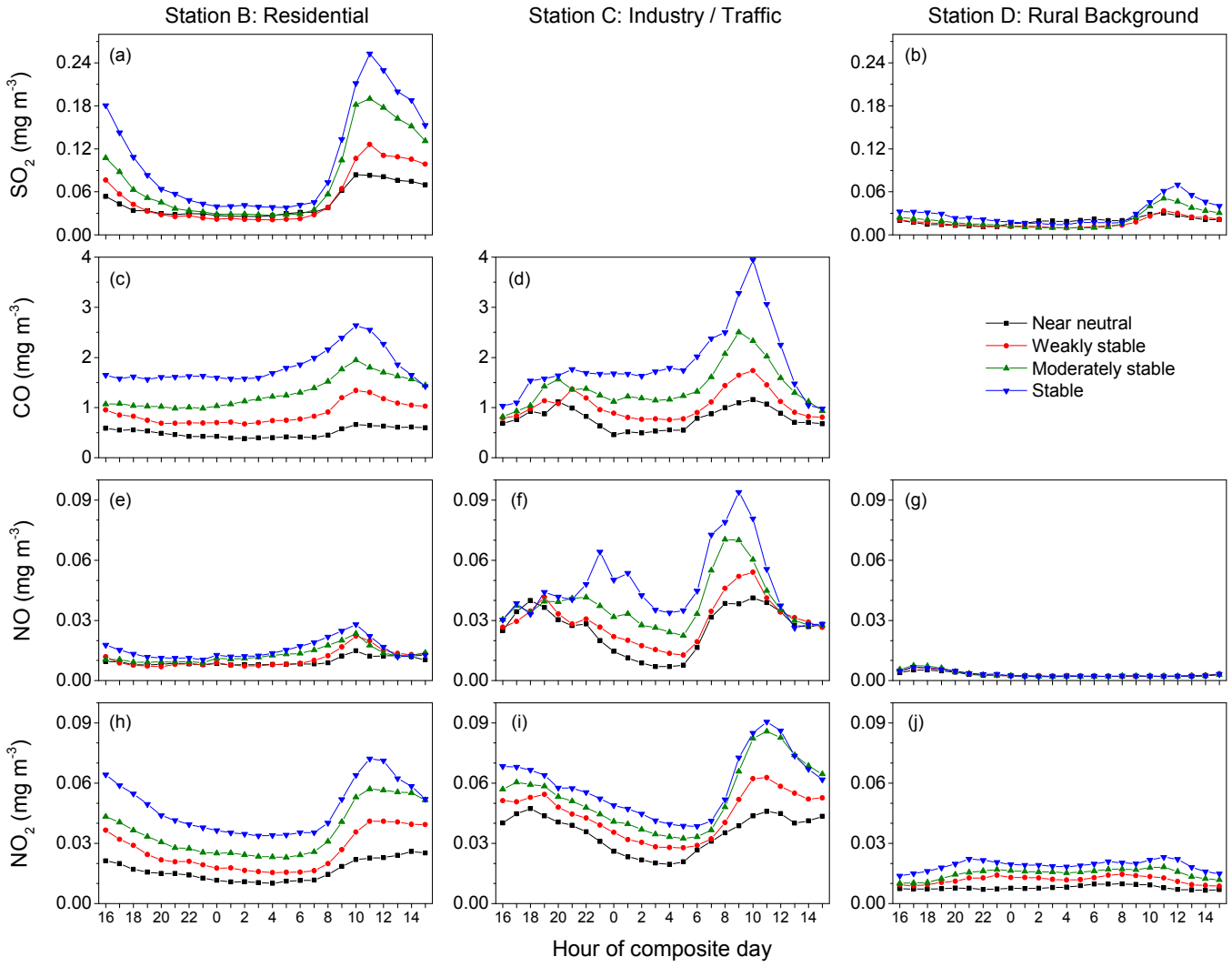

Fig. 12. Comparison of diurnal composite SO_2, CO, NO and NO_2 concentrations observed at Stations B, C and D as a function of radon-derived stability category.

scheme provides a consistent, gradual distinction in pollutant concentrations from near neutral to stable nocturnal conditions. Most notably, the diurnal amplitudes of pollutant concentrations are smallest when nocturnal conditions are near neutral, and largest when nocturnal conditions are stable. It should be noted here that summer conditions are under-represented compared to winter conditions for this 11-month dataset, and that a larger number of "stable" nights occurred in winter (when pollutant levels were generally higher) than summer (Fig. 10a). This has resulted in an increase in pollutant concentration during the afternoon with increasing nocturnal stability classification that is larger than would be expected if the seasonal data were pro-cessed separately.

Maximum pollutant concentrations are typically observed mid-morning when peak-hour emissions are released into a mixing layer that is not yet well developed. At Station C, close to a major roadway, a "double-peak" is observed. The second peak is most clearly evident in the early evening for primary pollutants (e.g. CO and NO) close to the main sources (e.g. at Station C), when peak-hour traffic emissions are being released into the developing stable nocturnal boundary layer. The NO peak observed between 2200 and 0000h corresponds to direct emissions from trucks, which are not allowed on the nearby road during the day.

Based on the results of this classification scheme, averaged over all seasons, a factor of 2–4 increase in mean pollutant concentration can be expected on the morning following a stable night compared to near neutral nocturnal conditions; larger increases would be expected for the winter-only case.

A strong gradient in pollutant concentrations from Station C (industrial/traffic) to Station D (rural background) is evident. In particular, a factor of seven difference is estimated between peak NOx concentrations in the industrial region and the rural background location under "stable" conditions.

4.4. Comparison with traditional stability classification measures

As discussed in the Introduction, and in Chambers et al.(2014b), the stability classification schemes traditionally used with routine climatological observations are the Pasquil-Gifford turbulence (PGT) and radiation (PGR) schemes. Chambers et al.(2014b) compared the radon-based and PGT classification schemes at an open, flat, inland Australian site. However, due to the low wind speeds characteristic of Lanzhou, the PGT classifi-cation scheme cannot be used. Consequently, the PGR scheme has been adopted as the Chinese National Standard (GB/T 13201-91) for stability typing in order to assess the air quality impact of

gaseous and particulate emissions. Since the focus of this study is nocturnal stability typing, we will consider only 3 of the 6 PGR stability categories for our comparison: **D** (near neutral), **E** (moderately stable), and **F** (stable).

We used CMA climatological observations to assign PGR stability classifications to the entire dataset at 6-hourly intervals (0200, 0800, 1400, 2000h). Next we assumed that the 0200h PGR stability classification was most representative of the nocturnal stability conditions each night, and formed diurnal composites of ΔRn^* based on these categories (Fig. 13).

Of the 335 nights potentially available in the 11-month dataset, there were 261 complete nights on which all observations (climatology, pollution, and radon) were available. A breakdown of how the radon-based and PGR schemes distributed the available observations between the assigned stability categories is provided in Table 1. Immediately evident is the highly uneven distribution of events between stability categories by the PGR scheme.

Comparing Fig. 13 to Fig. 8, we see that the PGR "F" (stable) category yields a similar nocturnal ΔRn^* accumulation pattern to the "Class 3" (moderately stable) radon-based category, and the "E" category matches similarly with the "Class 2" (weakly stable) radon-based category. However, the neutral PGR category ("D") exhibits a diurnal amplitude more than twice that of the near-neutral radon-based category, and is not clearly distinct from category "E". Furthermore, regarding the accumulation of emissions on the most stable of evenings, none of the PGR stability classifications accurately represent the degree of radon accumulation indicated by the "Class 4" (stable) events of the radon-based category. It therefore seems likely that all categories of the PGR scheme incorporate a large range of stability conditions as diagnosed by the radon-based scheme, and that extreme cases of both near-neutral and very stable nights are not well identified by the PGR scheme.

Next we reproduced Fig. 12 based on results of the PGR stability classifications (Fig. 14). It is evident that pollutant concentrations were not always as well resolved by the PGR classification scheme (e.g. Fig. 12d c.f. Fig. 14d), and peak pollutant concentrations under the most stable conditions were always underestimated compared to the radon-based scheme. Given that "Class 4" (stable) events according to the radon-based scheme account for a quartile (25%) of the observations (see Section 3.2), this indicates that mean pollutant concentrations derived with the PGR stability classification (Chinese National Standard used in modelling personal exposure) would frequently be underestimated in the case of extreme events.

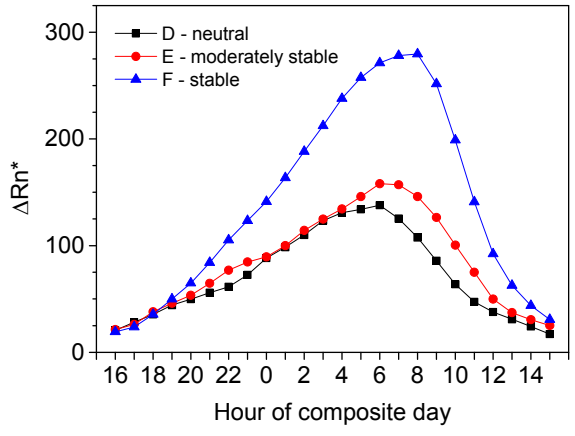

Fig. 13. Hourly-mean diurnal composite ΔRn^* values for PGR stability classifications D, E and F.

Table 1
Number of available nights (as a percentage) assigned to each stability classification by the two schemes.

Rn-based stability classification			PGR scheme stability classification		
Rn class	Stability	% of nights	PGR class	Stability	% of nights
1	Near neutral	20.7	D	Neutral	7.3
2	Weakly stable	33.3	E	Moderately stable	42.1
3	Moderately stable	29.5	F	Stable	50.6
4	Stable	16.5			

5. Conclusions

A recently-developed technique for radon-based nocturnal atmospheric stability classification is adapted for application to the SM200 "stability monitor". By isolating the diurnal (stability-related) contributions to the near-surface radon observations from the fetch-related (>diurnal time scale) components, the observations can be directly related to the atmospheric mixing state in a consistent way due to the spatial consistency of the "local" (several 10 s of km) radon source function.

We develop a 4-category nocturnal atmospheric stability classification scheme based on 11 months (July 2007—May 2008) of SM200 observations in Lanzhou, China, one of China's most polluted cities. Lanzhou is prone to atmospheric stagnation events, and has an annual mean wind speed of only 0.8 m s^{-1}. While these characteristics prevent the use of Pasquil-Gifford "turbulence" stability typing, the radon-based scheme was able to consistently distinguish between the 4 defined nocturnal stability classifications spanning a total wind speed difference of only 0.4 m s^{-1} from near neutral to stable tracer behaviour.

We applied the radon-based scheme to a suite of urban emissions (including SO_2, CO, NO and NO_2) from three well-separated sites of contrasting pollution characteristics (industrial, residential and rural background). Based on an annual composite there was a factor-of-three difference in SO_2 concentrations for the residential area between the least and most stable conditions, and a corresponding factor-of-four change in CO concentrations for both the residential and industrial areas. A factor of seven difference was estimated between peak NO_x concentrations in the city's industrial region and the rural background location under "stable" conditions.

This study concluded with a comparison of the radon-based and Pasquil-Gifford "radiation" stability classification schemes. The radon-based scheme was more successful at consistently distinguishing between states of atmospheric stability throughout the night and early morning than the PGR scheme, and could be employed completely independently of climatological observations. Our findings indicated that use of the PGR scheme could lead to underestimates of all pollutant concentrations under the most stable atmospheric conditions, in some cases (e.g. CO concentrations in the industrial region) by up to 25%.

A follow-up study is planned to investigate seasonal (warm/cold) characterisation of stability influences on primary and secondary urban pollutants in Lanzhou, and to better characterise winter extreme pollution events.

Acknowledgements

This study was supported by State Environmental Protection Key Laboratory of Sources and Control of Air Pollution Complex (No. SCAPC201404) and Laboratory for Climate Studies China Meteorological Administration Open Funds for Young Scholars (2014). The

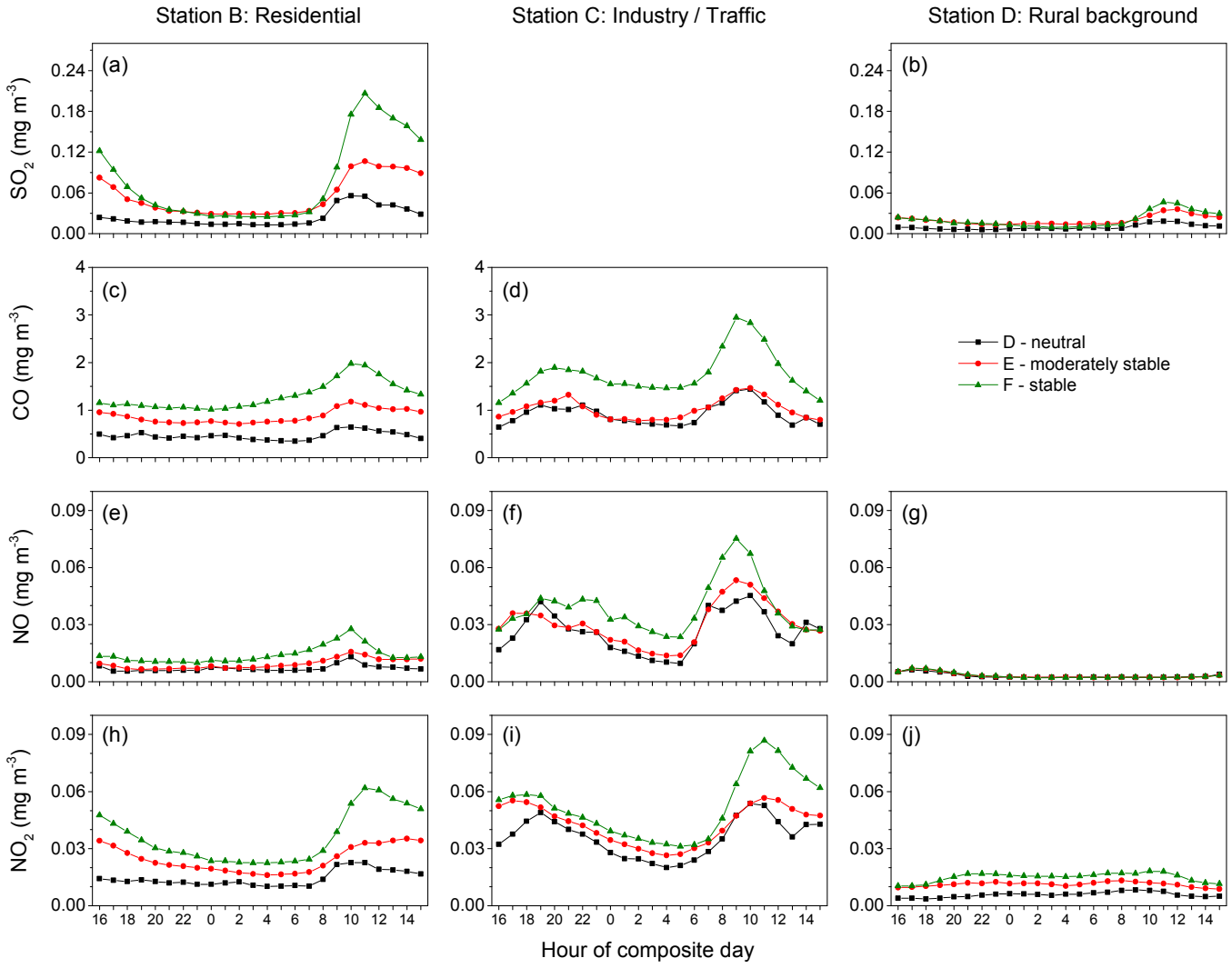

Fig. 14. Hourly-mean diurnal composite SO_2, CO, NO and NO_2 concentrations at Station B, C & D for PGR stability classifications D, E and F.

authors also thank the Sino-Italy environmental protection program-Air Quality Monitoring System (AQMS) supporting to obtain the data. The data used to generate the site map (Fig. 1) was sourced from Natural Earth (naturalearthdata.com), CGIAR-CSI SRTM version 4 (Jarvis et al., 2008), and Open Street Map (© OpenStreetMap contributors; www.openstreetmap.org/copyright).

References

Acevedo, O.C., Fitzjarrald, D.R., 2003. In the core of the night—effects of intermittent mixing on a horizontally heterogeneous surface. Bound. Layer Meteorol. 106, 1–33.

Allegrini, I., Febo, A., Pasini, A., Schiarini, S., 1994. Monitoring of the nocturnal mixed layer by means of participate radon progeny measurement. J. Geophys. Res. 99, 18765–18777. http://dx.doi.org/10.1029/94JD00783.

Avino, P., Brocco, D., Lepore, L., Pareti, S., 2003. Interpretation of atmospheric pollution phenomena in relationship with the vertical atmospheric remixing by means of natural radioactivity measurements (radon) of particulate matter. Ann. Chim. 93 (5–6), 589–594.

Begum, B.A., Biswas, S.K., Pandit, G.G., Saradhi, I.V., Waheed, S., Siddique, N., Seneviratne, M.C.S., Cohen, D.D., Markwitz, A., Hopke, P.K., 2011. Long–range transport of soil dust and smoke pollution in the South Asian region. Atmos. Pollut. Res. 2, 151–157.

Chambers, S., Zahorowski, W., Matsumoto, K., Uematsu, M., 2009. Seasonal variability of radon-derived fetch regions for Sado Island, Japan, based on 3 years of observations: 2002–2004. Atmos. Environ. 43, 271–279.

Chambers, S.D., Hong, S.-B., Williams, A.G., Crawford, J., Griffiths, A.D., Park, S.-J., 2014a. Characterising terrestrial influences on Antarctic air masses using radon-222 measurements at King George Island. Atmos. Chem. Phys. 14, 9903–9916. http://dx.doi.org/10.5194/acp-14-20 9903–2014.

Chambers, S.D., Williams, A.G., Crawford, J., Griffiths, A.D., 2014b. On the use of radon for quantifying the effects of atmospheric stability on urban emissions. Atmos. Chem. Phys. Discuss. 14, 25411–25452. http://dx.doi.org/10.5194/acpd-14-25411-2014.

Chan, C.K., Yao, X.H., 2008. Air pollution in mega cities in China. Atmos. Environ. 42 (24), 1–42.

Chinese Ministry of Environmental Protection, 2014. China Environmental Report 2013. China Environmental Report, Beijing.

Conen, F., Robertson, L.B., 2002. Latitudinal distribution of radon-222 flux from continents. Tellus 54B, 127–133.

Desideri, D., Roselli, C., Feduzi, L., Meli, M.A., 2006. Monitoring the atmospheric stability by using radon concentration measurements: a study in a central Italy site. J. Radioanal. Nucl. Chem. 270, 523–530.

Di Carlo, P., Pitari, G., Mancini, E., Gentile, S., Pichelli, E., Visconti, G., 2007. Evolution of surface ozone in central Italy based on observations and statistical model. J. Geophys. Res. 112, D10316,. http://dx.doi.org/10.1029/2006JD007900.

Duenas, C., Perez, M., Fernandez, M.C., Carretero, J., 1996. Radon concentrations in surface air and vertical atmospheric stability of the lower atmosphere. J. Environ. Radioact. 31, 10 87–102.

Foken, T., 2008. Micrometeorology. Springer-Verlag, Berlin Heidelberg (ISBN 978-3-540-74665-2), 306 pp.

Galmarini, S., 2006. One year of ^{222}Rn concentration in the atmospheric surface layer. Atmos. Chem. Phys. 6, 2865–2887.

Guedalia, D., Ntsila, A., Druilhet, A., Fontan, J., 1980. Monitoring of the atmospheric stability above an urban and suburban site using sodar and radon measure-ments. J. Appl. Meteorol. 19, 839–848. http://dx.doi.org/10.1175/1520-0450(1980)019<0839:MOTASA>2.0.CO;2.

Griffiths, A.D., Parkes, S.D., Chambers, S.D., McCabe, M.F., Williams, A.G., 2013.

Improved mixing height monitoring through a combination of lidar and radon measurements. Atmos. Meas. Tech. 6, 207–218. http://dx.doi.org/10.5194/amt-6-207-2013.
Guttikunda, S.K., Thongboonchoo, N., Arndt, R.L., Calori, G., Carmichael, G.R., Streets, D.G., 2001. Sulfur deposition in Asia: seasonal behavior and contributions from various energy sectors. Water Air Soil Pollut. 131, 383–406.
He, K.H., Yang, F.M., Duan, F.K., 2011. Atmospheric Particulate Matter and Regional Complex Air Pollution. Science Press, Beijing, China.
Huebert, B.J., Bates, T., Russell, P.B., Shi, G., Kim, Y.J., Kawamura, K., Carmichael, G., Nakajima, T., 2003. An overview of ACE-Asia: strategies for quantifying the relationships between Asian aerosols and their climatic impacts. J. Geophys. Res. 108 (D23), 8633,. http://dx.doi.org/10.1029/2003JD003550.
Jarvis, A., Reuter, H.I., Nelson, A., Guevara, E., 2008. Hole-filled SRTM for the Globe Version 4, Available from the CGIAR-CSI SRTM 90m Database. http://srtm.csi.cgiar.org.
Ji, D., Li, L., Wang, Y., Zhang, J., Cheng, M., Sun, Y., Liu, Z., Wang, L., Tang, G., Hu, B., Chao, N., Wen, T., Miao, H., 2014. The heaviest particulate air-pollution episodes occurred in northern China in January, 2013: insights gained from observation. Atmos. Environ. 92, 546–556.
Ji, D., Wang, Y., Wang, L., Chen, L., Hub, B., Tang, G., Xin, J., Song, T., Wen, T., Sun, Y., Pan, Y., Liu, Z., 2012. Analysis of heavy pollution episodes in selected cities of northern China. Atmos. Environ. 50, 338–348.
Jo, H.Y., Kim, C.H., 2013. Identification of long-range transported haze phenomena and their meteorological features over Northeast Asia. J. Appl. Meteorol. Cli-matol. 52, 1318–1328.
Kan, H., Chen, R., Tong, S., 2012. Ambient air pollution, climate change, and population health in China. Environ. Int. 42, 10–19.
Kondo, H., Murayama, S., Sawa, Y., Ishijima, K., Matsueda, H., Wada, A., Sugawara, H., Onogi, S., 2014. Vertical diffusion coefficient under stable conditions estimated from variations in the near-surface radon concentration. J. Meteorol. Soc. Jpn. 92, 95–106. http://dx.doi.org/10.2151/jmsj.2014-106.
Mahrt, L., Vickers, D., Nakamura, R., Soler, M.R., Sun, J.L., Burns, S., Lenschow, D.H., 2001. Shallow drainage flows. Bound. Layer Meteorol. 101, 243–260.
Ministry of Environmental Protection of People's Republic of China, 2013 Report on the State of the Environment in China, 2014. http://jcs.mep.gov.cn/hjzl/zkgb/2013zkgb/.
Nie, W., Wang, T., Wang, W., Wei, X., Liu, Q., 2013. Atmospheric concentrations of particulate sulfate and nitrate in Hong Kong during 1995–2008: impact of local emission and super-regional transport. Atmos. Environ. 76, 43–51.
Ohara, T., Akimoto, H., Kurokawa, J., Horii, N., Yamaji, K., Yan, X., Hayasaka, T., 2007. An Asian emission inventory of anthropogenic emission sources for the period 1980–2020. Atmos. Chem. Phys. 7, 4419–4444.
Park, M.H., Kim, Y.P., Kang, C.-H., Shim, S.-G., 2004. Aerosol composition change between 1992 and 2002 at Gosan, Korea. J. Geophys. Res. 109, D19S13. http://dx.doi.org/10.1029/2003JD004110.
Perrino, C., February 2012. Natural Radioactivity from Radon Progeny as a Tool for the Interpretation of Atmospheric Pollution Events, Sources and Measurements of Radon and Radon Progeny Applied to Climate and Air Quality Studies. International Atomic Energy Agency, Vienna, Austria, pp. 151–159. ISBN 92-0-123610-4.
Pasquil, D., 1961. The estimation of the dispersion of windborne material. Meteorol. Mag. 90, 33–49.
Pasquill, F., Smith, F.B., 1983. Atmospheric Diffusion, third ed. Ellis Horwood Ltd., John Wiley & Sons, Chichester, p. 437.
Perrino, C., Pietrodangelo, A., Febo, A., 2001. An atmospheric stability index based on radon progeny measurements for the evaluation of primary urban pollution. Atmos. Environ. 35, 5235–5244.
Pitari, G., Coppari, E., De Luca, N., Di Carlo, P., 2014. Observations and box model analysis of radon-222 in the atmospheric surface layer at L'Aquila, Italy: March 2009 case study. Environ. Earth Sci. 71, 2353–2359. http://dx.doi.org/10.1007/s12665-013-2635-1.
Sesana, L., Caprioli, E., Marcazzan, G.M., 2003. Long period study of outdoor radon concentration in Milan and correlation between its temporal variations and dispersion properties of atmosphere. J. Environ. Radioact. 65, 147–160. http://dx.doi.org/10.1016/S0265-931X(02)00093-0, 25.
Sesana, L., Ottobrini, B., Polla, G., Facchini, U., 2006. 222Rn as indicator of atmospheric turbulence: measurements at Lake Maggiore and on the pre-Alps. J. Environ. Radioact. 86, 271–288. http://dx.doi.org/10.1016/j.jenvrad.2005.09.005.
Turner, B., 1964. A diffusion model for an urban area. J. Appl. Meteorol. 3, 83–91.
Vecchi, R., Marcazzan, G., Valli, G., 2007. A study on nighttime–daytime PM10 concentration and elemental composition in relation to atmospheric dispersion in the urban area of Milan (Italy). Atmos. Environ. 41, 2136–2144.
Wada, A., Murayama, S., Kondo, H., Matsueda, H., Sawa, Y., Tsuboi, K., 2010.Development of a compact and sensitive electrostatic radon-222 measuring system for use in atmospheric observation. J. Meteorol. Soc. Jpn. 88, 123–134.
Wang, F., Zhang, H., Ancora, M.P., Deng, X.-D., 2013a. Measurement of atmospheric stability index by monitoring radon natural radioactivity. China Environ. Sci. 33 (4), 594–598.
Wang, F., Zhang, Z., Ancora, M.P., Deng, X.-D., Zhang, H., 2013b. Radon natural radioactivity measurements for evaluation of primary pollutants. Sci. World J. http://dx.doi.org/10.1155/2013/626989.
Weller, R., Levin, I., Schmithüsen, D., Nachbar, M., Asseng, J., Wagenbach, D., 2013. On the variability of atmospheric 222Rn activity concentrations measured at Neumayer, coastal Antarctica. Atmos. Chem. Phys. Discuss. 13, 32817–32847. http://dx.doi.org/10.5194/acpd-13-32817-2013.
Williams, A.G., Chambers, S.D., Zahorowski, W., Crawford, J., Matsumoto, K., Uematsu, M., 2009. Estimating the Asian radon flux density and its latitudinal gradient in winter using ground-based radon observations at Sado Island. Tellus 61B, 732–746.
Williams, A.G., Chambers, S.D., Griffiths, A.D., 2013. Bulk mixing and decoupling of the nocturnal stable boundary layer characterized using a ubiquitous natural tracer. Bound. Layer Meteorol. 20 (149), 381–402. http://dx.doi.org/10.1007/s10546-013-9849-3.
Zahorowski, W., Chambers, S.D., Henderson-Sellers, A., 2004. Ground based radon-222 observations and their application to atmospheric studies. J. Environ. Radioact. 76, 3–33.
Zhang, K., Feichter, J., Kazil, J., Wan, H., Zhuo, W., Griffiths, A.D., Sartorius, H., Zahorowski, W., Ramonet, M., Schmidt, M., Yver, C., Neubert, R.E.M., Brunke, E.-G., 2011. Radon activity in the lower troposphere and its impact on ionization rate: a global estimate using different radon emissions. Atmos. Chem. Phys. 11, 7817–7838.
Zhang, J., Zhang, H., Yun, Y., Ren, C., 2014. Spatial and temporal variation of particulate matter and gaseous pollutants in 26 cities in China. J. Environ. Sci. 26 (1), 75–82.
Zhang, L., Chen, C., Murlis, J., 2001. Study on winter air pollution control in Lanzhou. Water Air Soil Pollut. 127, 351–372.
Zhang, Q., He, K., Huo, H., 2012a. Cleaning China's air. Nature 484, 161–162.
Zahorowski, W., Chambers, S., Wang, T., Kang, C.H., Uno, I., Poon, S., Oh, S.N., Wercqynski, S., Kim, J., Henderson-Sellers, A., 2005. Radon-222 in boundary layer and free tropospheric continental outflow events at three ACE-Asia sites. Tellus 57 (2), 124–140.
Zhang, Z., Wang, F., Costabile, F., Allegrini, I., Liu, F., Hong, W., 2012b. Interpretation of ground-level ozone episodes with atmospheric stability index measurement. Environ. Sci. Pollut. Res. 19, 3421–3429. http://dx.doi.org/10.1007/s11356-012-0867-3.